Enhanced Sulfate Formation in Mixed Biomass Burning and Sea-salt Interactions Mediated by Photosensitization: Effects of Chloride, Nitrogen-containing Compounds and Atmospheric Aging

Rongzhi Tang[1,2], Jialiang Ma[3], Ruifeng Zhang[4], Weizhen Cui[1], Yuanyuan Qin[5], Yangxi Chu[6], Yiming Qin[1], Alexander L. Vogel[3], Chak K. Chan[4,*]

[1] School of Energy and Environment, City University of Hong Kong, Hong Kong, China

[2] Shenzhen Research Institute, City University of Hong Kong, Shenzhen 518057, China

[3] Institute for Atmospheric and Environmental Sciences, Goethe-University Frankfurt, 60438 Frankfurt am Main, Germany

[4] Division of Physical Science and Engineering, King Abdullah University of Science and Technology (KAUST), Thuwal 23955-6900, Kingdom of Saudi Arabia

[5] College of Resources and Environment, University of Chinese Academy of Sciences, Beijing, 100049, China

[6] State Key Laboratory of Environmental Criteria and Risk Assessment, Chinese Research Academy of Environmental Sciences, Beijing, 100012, China

Correspondence to: Chak K. Chan (chak.chan@kaust.edu.sa)

Abstract

Discrepancies persist between modeled simulations and measured sulfate concentrations in marine boundary layer, especially when the marine air was influenced by biomass burning plume. However, there is a notable dearth of research conducted on the interactions between sea-salt aerosol and biomass burning plume, impeding a comprehensive understanding of the sulfate formation. This work studied sulfate formation by mixing real biomass burning (BB) extracts and NaCl, mimicking internal mixtures of BB and sea-salt particles. Significant enhancement of sulfate formation was observed for BB-NaCl particles compared to incense burning (IS)-NaCl particles. For fresh particles, the sulfate formation rate followed the trend of corn straw (CS)-NaCl>rice straw (RS)-NaCl>wheat straw (WS)-NaCl>IS-NaCl. The filter aging was achieved by exposing them to $OH^{\bullet}$ through UV irradiation. Aged particles showed changes in sulfate formation rates, with the highest enhancement by RS-NaCl due to interactions between RS and NaCl. Model experiments spiked with nitrogen-containing organic compounds (NOCs), such as pyrazine (CHN) and 4-nitrocatechol (CHON), revealed positive effects of chloride in the PS-CHON system and negative effects in the PS-CHN system. Our work suggests that BB reaching or near coastal areas could affect sulfate formation via photosensitizer-mediated reactions, potentially exacerbating air quality concerns.

Keywords: sulfate formation, biomass burning, photosensitization, sea-salt aerosol, chloride

1 Introduction

Recent fire outbreaks in areas like Canada, Amazonia, and Southeast Australia, together with the increased fire frequency and intensity reports in areas like western US have highlighted the risks of fire, especially biomass burning (BB), to human health and climate change (Bond et al., 2013; Andreae, 2019; Jones et al., 2022). As an agricultural powerhouse, China boasts immense agricultural crop yields, especially in rice, wheat, and corn throughout the country. These crop residues are frequently burned in rural areas for cooking and heating purposes, as well as for land preparation after harvest, resulting in the substantial production of light-absorbing species, such as brown carbon (BrC) (Chen et al., 2017). Recent studies have reported that specific BrC species from biomass burning, including vanillin (VL), acetovanillone, syringaldehyde (SyrAld), can act as photosensitizers (PS) and oxidize SO_2 to sulfate (Zhou et al., 2023; Liang et al., 2024). Atmospheric processes like aging or long-range transport, can alter the chemical compositions and optical properties of PS, potentially affecting the sulfate formation potential. Sea-salt aerosol (SSA), with its high particulate matter loadings and extensive surface area, plays a significant role in interfacial and multiphase reactions with reactive gases, thereby impacting global radiation balance and air quality in marine and coastal areas (Gantt and Meskhidze, 2013; Chi et al., 2015). Prior research has identified several secondary sulfate formation pathways in SSA, e.g., multiphase SO_2 oxidation by O_3 (Alexander et al., 2012), coexistence of NO_2 (Zhang and Chan, 2023b), PS (Tang et al., 2023), chlorine-PS synergistic effects (Zhang and Chan, 2024), and Cl and OH radicals generated by chlorine photoactivation (Cao et al., 2024), highlighting the importance of NaCl-based photochemistry in sulfate formation.

SSA can frequently mix with organic matter through processes such as sea-to-air emission, photochemical oxidation and atmospheric transport (Liu et al., 2023b). Previous studies have observed elevated sulfate concentrations in coastal regions when air masses passed through inland areas due to intensive BB or other anthropogenic emissions, suggesting the possible interactions between the SSA (primarily sodium chloride) and anthropogenic emissions (Qiu et al., 2019; Huang et al., 2018; Wu et al., 2022). Van Pinxteren et al. (2015) observed an increase in sulfate concentration (2.26 μg m^{-3}) during the RV MARIA S cruise as it approached the African mainland, in contrast to the marine-origin aerosol (1.59 μg m^{-3}), showing significant influence of BB. Hence, mixing of sea-salt and biomass burning aerosols can happen in coastal regions.

Since the sulfate formation rate depends on the intrinsic properties of the solution matrix and the two main reaction matrixes in marine boundary layer (MBL) were wet aerosol (droplet in our case) and cloud/fog (bulk aqueous), both droplet and aqueous reactions are relevant for studying the aqueous reactions in aerosols and clouds within MBL (Ruiz-Lopez et al., 2020; Herrmann, 2003). Typically, droplet experiments were characterized by high ionic strength (up to >10 M), low liquid water content (10^{-7}-10^{-3} cm^3 m^{-3}) and high surface-to-volume ratio whereas aqueous reactions exhibit the opposite characteristics. Transmission electron microscopy (TEM) studies indicate that most coastal particles are internally mixed, showing a higher proportion of organic and salt mixtures in the presence of biomass burning aerosols, accompanied by an increase in sulfate (Dang et al., 2022; Li et al., 2003) However,

discrepancies persist between modeled simulations and measured sulfate concentrations in MBL (Yu et al., 2023). The interactions of sea-salt and BB aerosols, especially in multiphase reactions, can potentially unravel the intricate chemistry of sulfate formation in BB affected MBL. Hence, internal mixtures of inorganic salt and water-soluble organic carbons are often used in reaction studies (Tan et al., 2024).

In this study, we performed in-situ droplet and aqueous experiments using BB extracts-NaCl mixture to explore the possible interplay between biomass burning and marine aerosols in coastal areas. BB was derived from the burning of rice straw (RS), wheat straw (WS), and corn straw (CS) as well as incense burning (IS). The aims of this study are to: (i) compare the differences in sulfate formation among different kinds of BB-NaCl particles and BB extracts; (ii) examine the impacts of the atmospheric aging (OH• aging) on sulfate formation across different BB-NaCl particles and BB extracts; (iii) investigate the role of chloride ions in BB extracts mediated sulfate formation.

2 Material and methods

2.1 Burning experiments

Three types of commonly used biomass (RS, WS and CS) were cut into small, uniform pieces (~10 cm in length) and dried. About 100 g of the dried biomass materials (~10% moisture content) was then introduced into a traditional iron stove commonly used in rural areas (Figure S1). The stove was covered with a hood and the biomass was ignited using a propane lighter. The generated BB smoke was collected onto 90-mm quartz filters at 0.9 m^3 min^{-1} for 10 minutes by a custom-made aerosol sampler under mixed combustion condition (include flaming and smoldering, modified combustion efficiency MCE, $0.85 \leq \Delta[CO_2]/(\Delta[CO_2]+\Delta[CO]) \leq 0.95$) (Ting et al., 2018). The sampler was placed at a height of 1 meter above the ground and connected to a $PM_{2.5}$ sampling head through a sampling pump. For incense burning (IS), laboratory generated smoldering smoke was collected on 47-mm quartz filters at a flow rate of ~ 6.0 L min^{-1} for 80 min using a stainless-steel combustion chamber. Note that the different combustion modes of IS and BB are intentionally used to represent the real-world combustion conditions. Our previous study demonstrated that IS was representative of BB based on GC×GC chromatograms and pixel-based partial least squares discriminant analysis (Tang et al., 2023). Hereafter, we will use BB to represent both the real BB materials and the surrogate materials (IS) unless otherwise specified. After sampling, the collected BB samples (fresh BB) were wrapped by pre-baked aluminum foil (550 ℃ for 6 h) and stored at -20 ℃ until further analysis.

To achieve atmospheric OH• aging, the collected fresh BB filter samples were placed in a pre-flushed combustion chamber (zero air, more than 24 h) and illuminated with UV lamps for 40 min. We used lamps of 185 nm and 254 nm, the combination of which have been widely used in oxidation flow reactor design and experiments for mimicking atmospheric OH• concentrations (Peng and Jimenez, 2020; Rowe et al., 2020; Tkacik et al., 2014; Hu et al., 2022). The estimated OH exposure was $\sim 2.0\times10^{12}$ molecules cm^{-3} s, equivalent to an atmospheric aging period of 15 days (assuming an average atmospheric OH concentration of 1.5×10^6 molecules cm^{-3}) (Mao et al., 2009). Detailed characterization of the OH exposure can be found in our previous study (Tang et al., 2023).

2.2 Materials and instrumentation

Aqueous stock solutions of BB samples were prepared by dissolving the collected filters in ultrapure water and subjecting them to ultrasonication in a cooled-water bath three times, each for 20 minutes. The resulting water extracts of the BB were then filtered through 0.22 μm PTFE filters and stored in brown vials at 4℃ in a refrigerator. The anions, i.e., chloride, sulfate and nitrate of the BB extracts were analyzed by Dionex ion chromatography (ICS 1100, CA). An aliquot (~0.5 ml) of the BB or IS extracts were used for water-soluble organics detection by ultra-high performance liquid chromatography (Thermo Scientific Dionex UltiMate 3000 UHPLC) coupled with high-resolution Orbitrap Fusion Lumos Tribrid mass spectrometry (Orbitrap HRMS, Thermo Fisher Scientific, USA). The particulate organic matter was also characterized by a thermal desorption module (TDS3, Gerstel) coupled to comprehensive two-dimensional gas chromatography-mass spectrometer (GCMS-TQ™8050 NX, Shimadzu, Japan). UV-Vis spectrometry (UV-3600, Shimadzu, Japan) was employed to examine the absorbance of BB extracts. Total organic carbon (TOC) was measured by total carbon analyzer (TOC-L CPH, Shimadzu, Japan). Metal concentrations were measured by inductively coupled plasma-mass spectrometry (ICP-MS, Agilent 7800). Detailed analysis can be found in Text S1. Aqueous stock solution of sodium chloride (≥99.8%, Unichem) was prepared by dissolving the corresponding salt in ultrapure water to obtain a concentration of 1M. The study utilized high purity grade synthetic air and nitrogen supplied by the Linde HKO Ltd., while sulfur dioxide was obtained from the Scientific Gas Engineering Co., Ltd.

2.3 Multiphase and aqueous-phase reactions of S(IV)

In SO_2 uptake experiments, the stock solution of BB extracts was premixed with sodium chloride solution (1M) at a volume ratio of 1:1 and the solutions had pH a of 4-6. A droplet generator (Model 201, Uni-Photon Inc.) was then utilized to deposit droplets onto a hydrophobic substrate (model 5793, YSI Inc.) for SO_2 uptake experiments. Reactive SO_2 uptake experiments were performed via a flow cell/in-situ Raman system at controlled room temperature (23-25℃). The top and bottom quartz windows of the flow cell were used for Raman analysis and UV irradiation, respectively. The light experiment was performed using a xenon lamp (model 6258, ozone free, 300W, Newport, light intensity of 1318 mW/cm^2), with photon flux of 9.8 $\times 10^{15}$ photons cm^{-2} s^{-1} in 280-420 nm received by particles in the flow cell (Zhang and Chan, 2023b). Identical experiments were conducted in the dark, with the lights off and the experimental area kept in complete darkness. The relative humidity (RH) inside the flow cell was adjusted to 80% by mixing dry and wet synthetic air or nitrogen. The particles were then equilibrated at 80% RH for over 60 min and remained liquid throughout the experiment period. SO_2 was introduced into the system to reach a concentration of 8.0 ppm. The prescribed size used in our in-situ Raman research was 60 ± 5 μm. Despite using particles for droplet experiments that were larger than ambient fine particles, we employed the SO_2 uptake coefficient (γ_{SO_2}) as a kinetic parameter to account for the particle size effects. Comprehensive calculation of γ_{SO2} can be found in our previous studies (Gen et al., 2019a, b; Tang et al., 2023; Zhang et al., 2020a).

Aqueous-phase photochemical reactions were performed using a custom-built quartz photo reactor (Mabato et al., 2023; 2022). Specifically, a 500 mL solution containing 100 ppm

bisulfite and 1 ppm BB TOC extracts were continuously mixed using a magnetic stirrer throughout the experiments. Note that the 1 ppm BB TOC and 100 ppm bisulfite align well with the atmospheric-relevant ranges in aqueous aerosols, fogs and clouds, where PS concentration can reach hundreds of micromolar and total sulfur concentration can exceed several millimolar (Anastasio et al., 1997; Guo et al., 2012; Shen et al., 2012; Rao and Collett, 1995). To achieve air-saturated conditions, synthetic air was continuously introduced to the solutions at a flow rate 0.5 L min^{-1} throughout the experiments. The above mixed solutions were then exposed to radiation via the same xenon lamp as in the droplet experiments. Samples were collected at 1h interval for a total of 8 h for sulfate and bisulfite analysis using ion chromatography.

3 Results and Discussion

3.1 Enhanced sulfate production of BB-NaCl droplets compared to IS-NaCl droplets.

As no sulfate was detected in the dark conditions for any of the experiments, we have focused on the light experiments. Figure 1 depicts the sulfate production by (a) fresh BB-NaCl; (b) aged BB-NaCl droplets as a function of time in the presence of light, air and SO_2 at 80% RH. As our previous study (Tang et al., 2023) has found significantly higher sulfate formation of IS-NaCl droplets over NaCl droplets, here we only focus on the comparison of sulfate formation between different kinds of BB-NaCl droplets and IS-NaCl droplets. Regardless of whether the extracts were fresh or aged, the sulfate production by real BB-NaCl droplets was higher than IS-NaCl droplets. Specifically, sulfate formed by fresh (F) BB-NaCl droplets followed the trends of CS_F-NaCl (16.8 ± 2.6 mM $ppmC^{-1}$) >RS_F-NaCl (9.8 ± 0.1mM $ppmC^{-1}$) >WS_F-NaCl (4.2 ± 0.2mM $ppmC^{-1}$) >IS_F-NaCl (0.8 mM $ppmC^{-1}$) after illumination for 1080 min. In aged (A) samples, while BB_A-NaCl is more efficient than IS_A-NaCl in sulfate formation, the order of sulfate formation was different from the fresh samples: RS_A-NaCl (35.2 ± 0.6 mM $ppmC^{-1}$) > CS_A-NaCl (13.0 ± 0.1 mM $ppmC^{-1}$) > WS_A-NaCl (6.0 ± 1.6 mM $ppmC^{-1}$) > IS_A-NaCl (0.6 mM $ppmC^{-1}$). The sulfate enhancement factors of RS_F-NaCl, WS_F-NaCl, and CS_F-NaCl over IS_F-NaCl after 18 h SO_2 uptake ($Sulfate_{BB_F-NaCl/IS_F-NaCl}$) were 11.7, 5.0 and 20.0, respectively. The enhancement of sulfate can also be observed in aged BB samples, with values of 54.3, 9.2 and 20.1 for RS_A-NaCl, WS_A-NaCl, and CS_A-NaCl, respectively. The lower sulfate formation of IS-NaCl droplets than BB-NaCl droplets can be explained by the significantly higher TOC concentration of IS due to the incomplete and smoldering combustion (Table S1). The TOC concentration of the IS extracts (>550 mg L^{-1}) was nearly an order of magnitude higher than that of the BB extracts (34.0-69.9 mg L^{-1}), while WSOC/(WSOC+∑anions) exhibited a more than tenfold increase in BB extracts than in IS extracts. Previous studies have confirmed that the smoldering condition of BB will result in significantly more organic compounds and less ions than flaming condition (Wang et al., 2020b; Fushimi et al., 2017; Kalogridis et al., 2018; Kim et al., 2018). Additionally, significantly higher polycyclic aromatic hydrocarbons (PAHs) proportion (12.2%-16.6% by intensity) than IS (~5.0%) were observed by GC×GC-MS. Huang et al. (2022a) reported higher PAHs in BB particulates (CS, WS, RS, >262.5 mg kg^{-1}, >3.7% of organic matter) than in IS particulates (3.3 mg kg^{-1}, 0.9% of organic matter) (Song et al., 2023). Fushimi et al. (2017) and Kim et al. (2021) demonstrated that more PAHs would be emitted

under flaming compared to smoldering conditions. PAHs like pyrene, fluoranthene, and phenanthrene have been recognized as PS(Jiang et al., 2021; Yang et al., 2021) and are mainly from combustion processes, e.g., pyrosynthesis from aliphatic and aromatic precursors in biomass burning processes and the constituents vary with temperatures and oxygen contents (Pozzoli et al., 2004). The higher percentage of PAHs in BB together with the collection procedure (mixed combustion and higher temperature for real BB while smoldering and lower temperature for IS) suggested the BB materials would generate more PAHs at high temperatures and may contribute to sulfate formation.

Table 1 and Figure S2 presents the reactive (γ_{SO_2}) and normalized reactive SO_2 uptake coefficients ($n\gamma_{SO_2}$) of different BB-NaCl droplets. The γ_{SO_2} obtained in our study are 0.9 - 6.6×10^{-6}, which are consistent but fall on the low side of the reported heterogeneous SO_2 oxidation processes, including nitrate photolysis (10^{-6}-10^{-5}) (Gen et al., 2019a), TMI-catalyzed oxidation (10^{-6}-10^{-4}) (Zhang et al., 2024), NO_2/O_3 oxidation (10^{-6}-10^{-4}) (Zhang et al., 2021a; Zhang and Chan, 2023a) and peroxide oxidation (10^{-6}-10^{-1}) (Wang et al., 2021; Ye et al., 2018; Yao et al., 2019). Additionally, the reported γ_{SO_2} in our study aligns well with the results obtained from ambient samples in Beijing (Zhang et al., 2020b). The large discrepancy of the reported γ_{SO_2} can be attributed to the differences in aerosol components, particle size, RH, SO_2 and oxidants concentrations. From our results, it appears that sulfate formation from BB-NaCl particles is much less effective than particles under nitrate photolysis. It is interesting to note that Zhou et al. (2023) found particles coated with model PS compounds much more effective in sulfate formation than nitrate particles under photolysis in a PAM reactor. The much shorter residence time in that reactor (2.5 min) and higher PS concentration (~66 mM) than the exposure time of filter samples (40 min) and PS concentration (<250 ppm) in our sulfate experiments may explain the differences in the comparison of PS/BB and nitrate photolysis results. Higher $n\gamma_{SO_2}$ were found for fresh and aged real BB-NaCl than IS-NaCl droplets, following the trend of :CS_F-NaCl (8.8×10^{-8} $ppmC^{-1}$)>RS_F-NaCl (6.2×10^{-8} $ppmC^{-1}$)>WS_F-NaCl (2.0×10^{-8} $ppmC^{-1}$)>IS_F-NaCl (0.61×10^{-8} $ppmC^{-1}$) and RS_A-NaCl (2.2×10^{-7} $ppmC^{-1}$)>CS_A-NaCl (6.2×10^{-8} $ppmC^{-1}$)>WS_A-NaCl (3.5×10^{-8} $ppmC^{-1}$)>IS_A-NaCl (0.46×10^{-8} $ppmC^{-1}$), respectively.

In our previous study, we observed a significant increase in sulfate formation for IS-NaCl droplets than NaCl droplets, which we attributed to photosensitization (Tang et al., 2023). Considering the fact that BB-NaCl droplets produced sulfate more efficiently than IS-NaCl droplets and NaCl droplets, we explore the underlying mechanisms driving this phenomenon. Possible reasons include nitrate (from BB extracts or newly formed) photolysis, [Cl^--H_3O^+-O_2] photoexcitation (Cl^- from BB extracts), H_2O_2 oxidation, BC-catalyzed oxidation, reactive nitrogen species oxidation, and organics-driven pathways e.g., HCHO, photosensitizing components, organic peroxide, and TMI-organic oxidation (Ye et al., 2023).

Since there was no nitrate peak in our Raman spectra in all experiments, the potential impact from nitrate photolysis was excluded. Besides, the significantly low Cl^- concentration (0.0002-0.001M) in the original BB extracts (compared to 1M NaCl, Table S1) has minimized the influence of chloride photoexcitation of [Cl^--H_3O^+-O_2] (Cl^- from BB extracts) on the sulfate formation. Reactive nitrogen species e.g., NO_x, HONO and NH_3 were neither introduced nor

detected in our system, indicating that the oxidation pathway involving reactive nitrogen species was insignificant. Additionally, the water extraction process has excluded the possibility of BC-catalyzed oxidation. The absence of sulfate formation in dark conditions ruled out the involvement of direct H_2O_2 oxidation and organic peroxide oxidation pathways. The concentrations of TMI did not exhibit a consistent relationship with the sulfate formation observed in both BB_F-NaCl and BB_A-NaCl droplets (Figure S3), suggesting that the TMI-catalyzed oxidation pathway may not be responsible for the observed phenomenon. Therefore, the most probable reason for the enhancement of sulfate formation by BB-NaCl droplets over NaCl droplets would be the photosensitizing components. Given the complexity and the lack of a method to quantify PS in BB aerosols, using the total TOC concentration as an upper limit for estimating PS concentration is considered a compromise that allows for systematic comparison. Our goal is to compare the photosensitizing ability in different chemical systems, but not to quantify their absolute values. Therefore, the sulfate formation reported here can be considered as the lower limit of photosensitizing capacity. State-of-the-art mass spectrometry analysis including UHPLC-Orbitrap-MS and GC×GC-MS showed the existence of possible PS such as PAHs (e.g., fluoranthene, pyrene, cyclopenta[cd]pyrene, 4-methylphenanthrene, benzo[a]pyrene, perylene, Table S2) and aromatic carbonyls (SyrAld, VL, 3,4-dimethoxybenzaldehyde, acetophenone, acetosyringone, Table S2). Photosensitizing components can directly or indirectly (by forming secondary oxidants in the presence of oxygen) oxidize S(IV) to S(VI). Wang et al. (2020a) proposed a direct oxidation process of S(IV) to sulfate by excited triplet states of photosensitizers (^{3}PS*). To explore the contribution of the direct ^{3}PS* oxidation on sulfate formation, we performed the same sets of experiments in N_2-saturated condition, shown in Figure 2. Under N_2-saturated conditions, secondary oxidants such as HO_2•, OH• oxidation pathway can be ruled out due to the lack of oxygen. Consequently, the sulfate formed under this condition can be considered as the direct PS* oxidation. The BB-NaCl droplets showed only direct PS* oxidation contribution of 3.6% to 22.7%, highlighting the predominant role of secondary oxidants (Tang et al., 2023). For BB_F-NaCl droplets, the contribution of direct PS* followed the trend of WS_F-NaCl (22.7%) > RS_F-NaCl (15.7%) > CS_F-NaCl (7.0%), while for BB_A-NaCl droplets, WS_A-NaCl (10.2%) > CS_A-NaCl (6.7%) > RS_A-NaCl (3.6%) was observed. In summary, regardless of whether fresh or aged, the secondary oxidants triggered by indirect PS* oxidation were the main reason for sulfate formation, highlighting the importance of O_2 in PS* mediated oxidation processes.

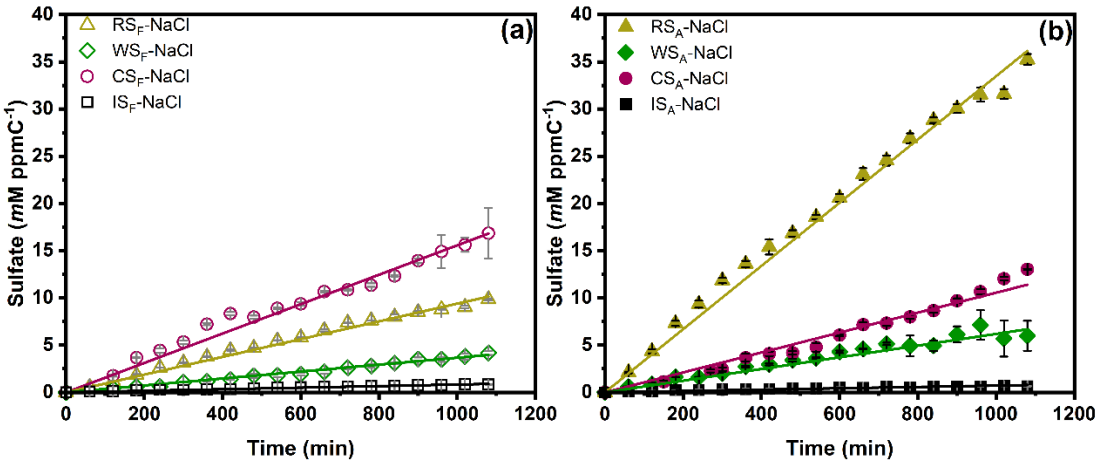

Figure 1. Sulfate production under different droplet compositions as a function of time by droplet experiments: (a) fresh BB-NaCl droplets; (b) aged BB-NaCl droplets in air at 80% RH. RS, WS, CS and IS represent rice straw, wheat straw, corn straw and incense burning, respectively. The subscripts F and A represent fresh and aged, respectively.

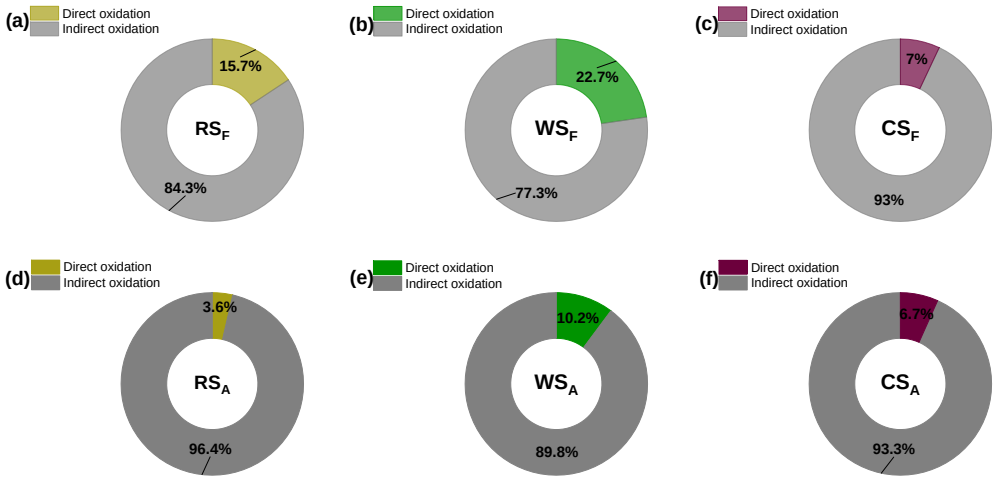

Figure 2 Contributions of direct and indirect PS* oxidation to sulfate in droplet experiments

Table 1. Sulfate formation rate constant ($k_{so_4^{2-}}$), reactive (γ_{SO_2}) and normalized SO_2 uptake coefficient ($n\gamma_{SO_2}$) of various particle compositions at 80% RH. Sulfate formation rate ($k_{so_4^{2-}}$) for aqueous phase reactions using different BB extracts and model compounds. 1, 10, 100 and 200 represent the concentration of different compounds (in ppm).

Particle Composition	$k_{so_4^{2-}}$ (μM min^{-1} ppmC^{-1})	γ_{SO_2}	$n\gamma_{SO_2}$ [a] ppmC^{-1}
RS$_F$-NaCl	9.4 ± 0.10	(2.2 ± 0.023)×10^{-6}	(6.2 ± 0.066)×10^{-8}
WS$_F$-NaCl	3.7 ± 0.048	(0.66 ± 0.0086)×10^{-6}	(2.0 ± 0.027)×10^{-8}
CS$_F$-NaCl	15.6 ± 0.11	(2.0 ± 0.015)×10^{-6}	(8.8 ± 0.065)×10^{-8}
IS$_F$-NaCl	0.83 ± 0.011	(1.7 ± 0.034)×10^{-6}	(0.61 ± 0.012)×10^{-8}
RS$_A$-NaCl	33.5 ± 0.38	(6.6 ± 0.074)×10^{-6}	(21.5 ± 0.24)×10^{-8}
WS$_A$-NaCl	6.2 ± 0.18	(0.92 ± 0.027)×10^{-6}	(3.5 ± 0.10)×10^{-8}
CS$_A$-NaCl	10.6 ± 0.23	(1.0 ± 0.023)×10^{-6}	(6.2 ± 0.13)×10^{-8}
IS$_A$-NaCl	0.72± 0.026	(1.3 ± 0.052)×10^{-6}	(0.46 ± 0.017)×10^{-8}

Aqueous Reactions	Concentration (ppm)	$k_{so_4^{2-}}$ (ppm min^{-1})	$k_{so_4^{2-}}$ [a] (μM min^{-1})
RS$_F$	1	0.31	3.2

RS_F-NaCl	1-100	0.16	1.6
RS_F-NaCl	1-200	0.085	0.9
WS_F	1	0.19	2.0
CS_F	1	0.25	2.6
IS_F	1	0.19	2.0
RS_A	1	0.33	3.4
RS_A-NaCl	1-100	0.37	3.8
RS_A-NaCl	1-200	0.63	6.4
WS_A	1	0.26	2.7
CS_A	1	0.33	3.4
IS_A	1	0.080	0.82
NaCl	100	0.051	0.52
NaCl	200	0.079	0.81
SyrAld	1	0.15	1.5
SyrAld-Pyz	1-1	0.68	7.1
SyrAld-Pyz-NaCl	1-1-10	0.67	6.9
SyrAld-Pyz-NaCl	1-1-100	0.55	5.7
SyrAld-Pyz-NaCl	1-1-200	0.50	5.2
SyrAld-4-NC	1-1	0.11	1.1
SyrAld-4-NC-NaCl	1-1-10	0.13	1.4
SyrAld-4-NC-NaCl	1-1-100	0.13	1.4
SyrAld-4-NC-NaCl	1-1-200	0.15	1.5
SyrAld-NaCl	1-10	0.11	1.1
SyrAld-NaCl	1-100	0.17	1.8
SyrAld-NaCl	1-200	0.17	1.7
VL	1	0.26	2.7
VL-Pyz	1-10	0.61	6.4
VL-Pyz-NaCl	1-1-10	0.55	5.8
VL-Pyz-NaCl	1-1-100	0.43	4.5

VL-Pyz-NaCl	1-1-200	0.42	4.3
VL-4-NC	1-1	0.17	1.7
VL-4-NC-NaCl	1-1-10	0.22	2.3
VL-4-NC-NaCl	1-1-100	0.27	2.7
VL-4-NC-NaCl	1-1-200	0.23	2.4
VL-NaCl	1-10	0.25	2.6
VL-NaCl	1-100	0.26	2.7
VL-NaCl	1-200	0.28	2.9

[a]The $n\gamma_{SO_2}$ was calculated by normalizing the γ_{SO_2} with the TOC concentration in the BB extracts, i.e., $n\gamma_{SO_2} = \gamma_{SO_2}/TOC$

3.2 Aging effects on sulfate formation across various BB materials

To investigate the aging effects across various BB materials, we subjected the collected BB filters to OH radical aging by irradiating them with UV lights at wavelengths of 185 nm and 254 nm. This combination effectively generate OH radicals (Tang et al., 2023). Figure S4 exhibits the differences in sulfate formation rates of different fresh and aged BB materials. RS and WS show sulfate formation enhancement, while CS and IS show reduction after aging. Figure 3(a) shows that the 18h sulfate enhancement factor ($Sulfate_A/Sulfate_F$) followed the trend of RS-NaCl (3.6) >WS-NaCl (1.4) > CS-NaCl (0.8) ≈ IS-NaCl (0.8), which is neither consistent with the trends of sulfate formation for BB_F-NaCl nor BB_A-NaCl, indicating that aging processes have different influence on sulfate formation towards BB materials. A similar trend was found for $n\gamma_{SO_2}$, showing the highest and lowest sulfate enhancement for RS-NaCl (3.5) and IS-NaCl (0.7), respectively.

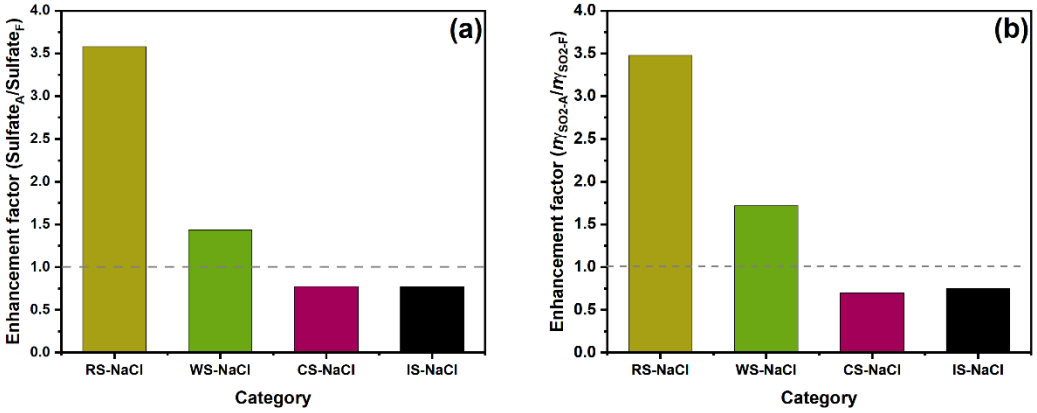

Figure 3. Enhancement factor of (a) sulfate and (b) normalized SO_2 uptake coefficient $n\gamma_{SO2}$ between fresh and aged BB-NaCl droplets by droplet experiments.

Aqueous reactions using fresh/aged BB extracts were performed to investigate the aging effects on the sulfate formation in cloud phase (Figure S5). As the experiment proceeded, sulfate

concentrations accumulated while bisulfite concentrations decreased. Concurrently, the pH of the aqueous solution decreased from approximately 5.0 to 3.0, reflecting enhanced acidity. In bulk experiments, all BB extracts have higher $k_{so_4^{2-}}$ after aging. The increased sulfate formation of BB extracts after aging may be due to changes in their chemical compositions. Compared to RS_F (28.3% for CHON- and 67.3% for CHN+ in total intensity), RS_A has higher CHON- (36.1%) and CHN+ (88.3%) percentages (Figs. S6-S7). Zhao et al. (2022) observed a slight increase in CHON percentage for RS from 53.4% to 56.2% after aging. Similar trend was observed for CS extracts, where CHON- and CHN+ percentage increases from 26.7% and 65.2% to 31.5% and 68.8%, respectively, after aging. Given the presence of chromophoric compounds in BrC (Laskin et al., 2015), we constrained the DBE values to the range of 0.5C≤DBE≤0.9C to semi-qualitatively distinguish BrC chromophores in the dissolved organic carbon (Lin et al., 2018). $BB_{F/A}$ was defined as the water-soluble organic species while $BB_{F/A\text{-}BrC}$ represented the molecularly identified water-soluble brown carbon falling in the range of $0.5C \leqslant DBE \leqslant 0.9C$ in BB extracts. These definitions will be consistently applied hereafter. Higher amounts of CHON- species were found in $RS_{A\text{-}BrC}$ (41.9%) and $CS_{A\text{-}BrC}$ (35.5%) than $RS_{F\text{-}BrC}$ (32.3%) and $CS_{F\text{-}BrC}$ (34.7%). One of the key categories of CHON- is nitrated aromatics, which have been widely identified in lab-generated BB smoke (Huang et al., 2022b; Wang et al., 2017a; Zhang et al., 2022; Xie et al., 2019) and field campaigns (Salvador et al., 2020; Mohr et al., 2013; Chen et al., 2022). A series of CHON- species, e.g., $C_6H_5NO_3$, $C_6H_5NO_4$, $C_7H_7NO_3$, and $C_8H_9NO_3$, which were tentatively identified as nitrophenol, nitrocatechol, methyl-nitrophenol, and dimethyl-nitrophenol, have been detected in our BB extracts. Nitrophenols photolysis has been found to be a potential source of OH radicals (Sangwan and Zhu, 2018; Guo and Li, 2023; Cheng et al., 2009; Sangwan and Zhu, 2016). Therefore, the increase in sulfate formation by RS_A and CS_A may partially be related to the more oxidants generated by nitrophenol photolysis.

Approximately 80% of the CHN+ species identified exhibited a diatomic nitrogen composition in their molecular formula. The precise determination of the molecular structures of these compounds solely based on elemental composition is challenging due to the presence of stable isomers. However, the N-bases, which contain two nitrogen atoms, can be attributed to various N-heterocyclic alkaloids (Figure S8). For example, homologs of $C_5H_6N_2(CH_2)_n$ were likely pyrazine, pyrimidine or amino pyridine, which were composed of six-membered heterocyclic rings with N atoms and alkyl side chains (Lin et al., 2012; Laskin et al., 2009). $C_5H_8N_2(CH_2)_n$ were likely alkyl-substituted imidazole compounds, featuring a five-membered heterocyclic ring with two nitrogen atoms as the core structure and alkyl side chains (Lin et al., 2012; Laskin et al., 2009). For $C_7H_6N_2(CH_2)_n$ homologs, the core skeleton was $C_7H_6N_2$, with an AI_{mod} of 0.8, indicating its distinctive characteristics of compounds containing fused five-membered and six-membered rings, such as benzimidazole or indazole (Wang et al., 2017b). Redox-inactive heterocyclic nitrogen-containing bases, e.g., pyridine, imidazole, and their derivatives, have been shown to enhance the redox activity of humic-like substances (HULIS) fraction by hydrogen-atom transfer, with the degree of enhancement directly correlated to their concentration (Dou et al., 2015; Kipp et al., 2004). Thus, the increased CHN+ percentage may also contribute to the enhanced sulfate formation of RS_A and CS_A by acting as a H-bond acceptor to facilitate the $^3PS^*$-mediated oxidation by generating more oxidants.

However, the CHON- and CHN+ percentages in WS_A were lower than WS_F, indicating that the

sulfate enhancement in WS_A was not due to the CHON and CHN species. Instead, CHO- accounted for higher proportion in WS_A (68.5%) and $WS_{A\text{-}BrC}$ (68.9%) than WS_F (65.0%) and $WS_{F\text{-}BrC}$ (64.8%).This aligns with a prior AMS study, showing increased CHO proportions in aged wheat burning emissions (Fang et al., 2017). We suppose that CHO- compounds, particularly photosensitizing compounds with carbonyl groups, would explain the difference of sulfate formation in WS extracts (Gómez Alvarez et al., 2012; Mabato et al., 2023; Felber et al., 2020; Fu et al., 2015). Therefore, we filtered the chemical formula of CHO- species from UHPLC-Orbitrap-HRMS by applying the maximum carbonyl ratio (MCR) (Zhang et al., 2021b; Wang et al., 2024a; Calderon-Arrieta et al., 2024; Liu et al., 2023a), H/C, O/C as well as modified aromaticity index (AI_{mod}) to focus on potential PS (Zherebker et al., 2022; Koch and Dittmar, 2006). In short, molecular formula were classified into six groups, namely, condensed aromatics ($AI_{mod}\geq0.67$), polyphenolics ($0.50<AI_{mod}<0.67$), highly unsaturated and phenolic compounds ($AI_{mod}\leq0.5$, $H/C<1.5$), aliphatics ($H/C\geq1.5$, $O/C\leq0.9$, $N=0$), peptide-like compounds ($H/C\geq1.5$, $O/C\leq0.9$, $N>0$) and sugar-like compounds ($H/C\geq1.5$, $O/C>0.9$), details can be found in Text S1. As aliphatics, peptide-like compounds and sugar-like compounds are unlikely to be PS, we exclude them as potential PS. By applying a data filtration process involving CHO-, condensed aromatics, polyphenolics, highly unsaturated and phenolic compounds based on the aforementioned criteria, as well as $MCR\geq0.9$ (which includes oxidized unsaturated and highly unsaturated compounds such as PS like imidazole-carboxaldehyde and PAHs) (Zhang et al., 2021b), 52.6% and 49.7% of the compounds (by intensity) can be considered as potential PS in WS_A and WS_F, respectively. The main compositional difference lies in polyphenolics, comprising 26.3% and 21.8% of WS_A and WS_F respectively. Therefore, the higher sulfate formation in WS_A may be related to the higher contributions of the polyphenolics, e.g., $C_8H_8O_3$.

To summarize, we propose that the enhanced sulfate formation in CS_A and RS_A was likely due to the increased proportions (by intensity) of CHON and CHN species, potentially nitrophenols and N-heterocyclic compounds. Conversely, the increased sulfate formation in WS_A appears to be linked to a higher percentage of CHO species. However, the associations between detailed chemical characteristics and sulfate formation were not provided in this study due to the complexity of the interactions between different chemical categories and difficulties in the interpretation of the coefficients. Future studies are needed to elucidate the relationships between sulfate formation and the chemical characteristics.

3.3 Effects of Chloride and Nitrogen-containing Species on Sulfate Formation

Unlike the droplet experiments where RS-NaCl has the highest sulfate enhancement factor after aging, aqueous reaction results (without NaCl) show a sulfate enhancement trend of WS>CS>RS>IS, suggesting that chloride may take effect in the droplet experiments, especially in RS-NaCl system. Therefore, bulk reaction experiments using RS extracts as an example were performed with 100-200 ppm NaCl additions, where the NaCl to TOC ratio ranged from 100:1 to 200:1 to match the 100:1 to 1000:1 range in droplet experiments, in order to evaluate the effects of chloride on sulfate formation. Interestingly, incorporating NaCl yielded contrasting results for RS_F and RS_A (Figure 4). While the addition of NaCl enhanced sulfate formation in RS_A, it showed the opposite trend in RS_F. The nature of the cations and ionic strength may

affect the sulfate formation rate; however, previous studies have indicated that their effects are negligible (Zhang and Chan, 2024; Parker and Mitch, 2016). The opposite effect of the NaCl addition on RS_F and RS_A, to some extent, explains the significantly higher sulfate and SO_2 uptake coefficient enhancement factor for RS-NaCl in Fig. 2. Compared to the RS-based system, NaCl control experiment showed minimum (but non-zero) sulfate formation (Table 1 and Figure 4). On one hand, it supported the findings that chloride participated in the sulfate formation under light but no sulfate formation under dark (Cao et al., 2024; Tang et al., 2023; Zhang and Chan, 2024). On the other hand, the opposite trend of Cl^- effects on RS_F and RS_A reflects its complex interactions with BB extracts under light and air. While direct reaction between S(IV) species and $^3PS^*$ may occur (Wang et al., 2020a), other pathways, i.e., interactions among halide ions, PS and oxygen should also be considered. PS in BB extracts can absorb solar radiation and form $^3PS^*$, which can then react with molecular oxygen and form singlet-state oxygen $^1O_2^*$ through energy transfer. $^3PS^*$ can also react with H-donor, typically organic acids (RH, e.g., vanillic acid, succinic acid, azelaic acid, glutaric acid, sorbic acid, salicylic acid, Table S3) through H transfer reactions, and form a ketyl radical (PSH•) and an alkyl or phenoxy radical (R•). PSH• and R• can then participate in a series of reactions to form OH•, HO_2•, H_2O_2 and $O_2^{\bullet-}$. In the presence of a large excess of Cl^-, Cl^- can act as an electron donor, and react with $^3PS^*$, forming a Cl• and a deprotonated ketyl radical (PS•) (Jammoul et al., 2009). Further reactions are similar to the abovementioned reactions, including the formation of reactive chlorine species (RCS, i.e., Cl•, $Cl_2^{\bullet-}$ and $ClOH^{\bullet-}$) and reactive oxygen species (ROS, i.e., OH•, HO_2•, H_2O_2 and $O_2^{\bullet-}$). These RCS and ROS simultaneously contribute to S(IV) oxidation to S(VI) (Zhang and Chan, 2024).

Statistical analysis using the Pearson correlation coefficient revealed that the concentrations of CHO, CHON, and CHN species exhibited significant correlations (|R|>0.5) with the sulfate formation rate ($p < 0.05$, Figure S9). As PS can be the main CHO species contributing to sulfate formation, N-containing organic compounds (NOCs), i.e., CHN and CHON species, may affect the chloride contribution on sulfate formation rate. Therefore, we selected SyrAld and VL as model CHO (PS), pyrazine (Pyz) as a model CHN, and 4-nitrocatechol (4-NC) as a model CHON to elucidate how potential chemical compounds can alter the effects of chloride on sulfate formation rate by studying the CHO+Cl^-, CHO+CHN+Cl^-, and CHO+CHON+Cl^- systems. For SyrAld and VL, as the $[Cl^-]_0/[PS]_0$ increases, $k_{so_4^{2-}}$ initially decreases and then increases. The initial decrease of $k_{so_4^{2-}}$ may be attributed to the quenching of $^3PS^*$ by electron transfer from Cl^- or loss of OH radials by forming $ClOH^{\bullet-}$ through reaction of OH•+Cl^- ↔$ClOH^{\bullet-}$(Anastasio and Newberg, 2007). Excessive chloride (e.g. 100 and 200 ppm) may generate Cl and OH radicals through photoexcitation in the presence of air and water and compensate for the loss of $^3PS^*$ or OH radicals. Previous studies have shown controversial influence of halides on the photosensitized oxidation of organic compounds or bisulfite. Parker and Mitch (2016) and Zhang et al. (2023) attributed the significantly higher photodegradation of dienes, thioethers and acetaminophen to the formation of reactive halogen species generated by the reactions of PS and halides. Zhang and Chan (2024) reported that $[Cl^-/PS]_0$ in the range of 1:2 to 4:1 did not lead to significant difference in sulfate formation, possibly due to the insufficient Cl^- concentration in triggering the interplay between PS and Cl^-. The differences between the current results and the aforementioned study might be attributed to the higher $[Cl^-/PS]_0$ (up to 1:200) which may have been sufficient to initiate the relevant reactions, as well as

the difference in photosensitizing capacities of the PS studied (triplet quantum yield of 0.86 ± 0.05 for 2-IC and 0.21 ± 0.01 for VL) (Felber et al., 2021; 2020). Safiarian et al. (2023) reported that increasing chloride concentrations facilitated anthracene photosensitization by producing high-level reactive oxygen species (ROS). Wang et al. (2023a) found that the effects of chloride on sulfate formation depended on the specific PS: enhancing sulfate production for benzophenone (BP) and 3,4-dimethoxybenzaldehyde (DMB), but decreasing it for 1,4-naphthoquinone.

When incorporating CHN species, a 2-3-fold $k_{so_4^{2-}}$ was observed, due to the enhanced H transfer by CHN acting as H-bond acceptor (Dou et al., 2015). With the addition of NaCl, the enhanced H-transfer effect by CHN was inhibited, possibly due to the consumption of ^{3}PS* by Cl^-. The addition of model CHON species into PS decreased $k_{so_4^{2-}}$, due to the consumption of ^{3}PS* by CHON species, in agreement with Wang et al. (2023b) who reported increased effective quantum yield of 4-NC when co-photolysis with VL. Further addition of NaCl increased the $k_{so_4^{2-}}$, possibly due to the consumption of 4-NC by RCS (Wang et al., 2024b), which, to some extent, reduced the loss of ^{3}PS*. Generally, the addition of chloride increased $k_{so_4^{2-}}$ of PS-CHON but decreased $k_{so_4^{2-}}$ of PS-CHN. However, the ambient air is characterized by the presence of tens of thousands of chemical compounds. As a result, the interplay among this diverse array of species may occur in ways that exceed current understanding, necessitating additional research to investigate the interactions between different organic compounds more thoroughly.

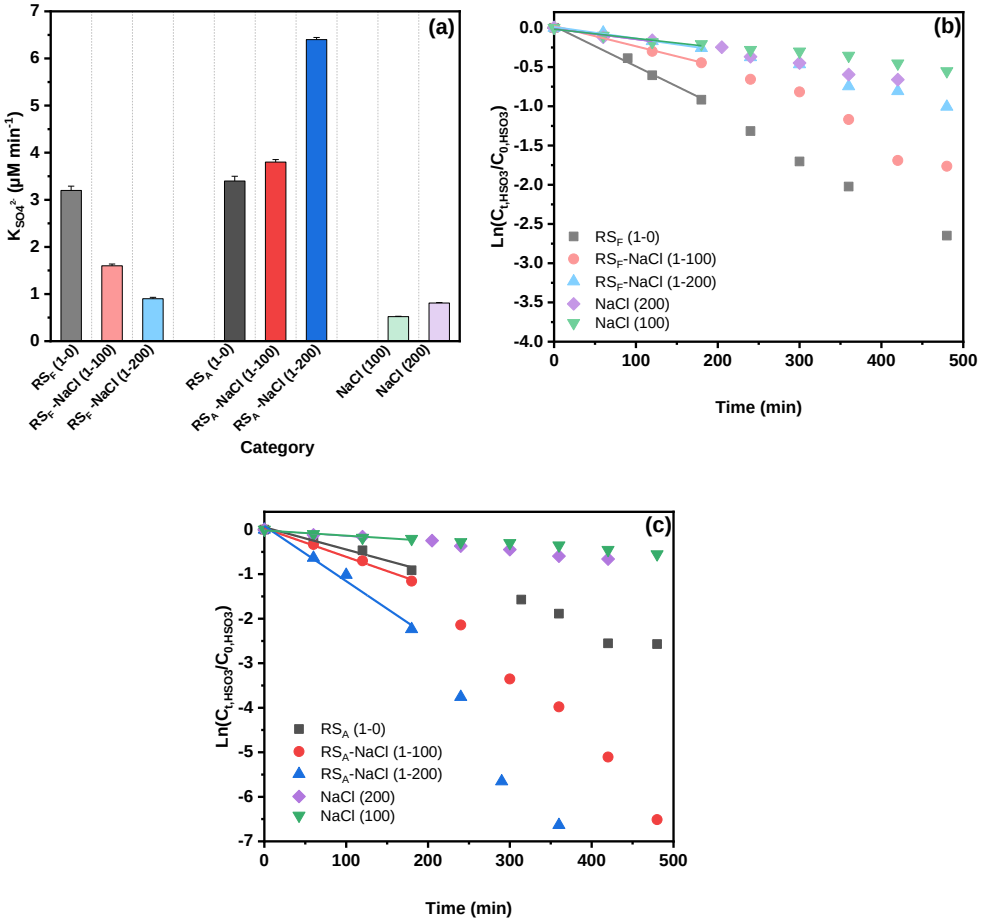

454

455 Figure 4. (a) Sulfate formation rate and (b) (c) bisulfite decay in RS-NaCl aqueous reactions. 1-0,
456 1-100, and 1-200 refer to the concentration ratios of TOC_{RS} and NaCl, in which 1, 100, 200 represent
457 1 ppm, 100 ppm and 200 ppm, respectively.

458 **3.4 Proposed mechanism for sulfate formation**

459 A conceptual diagram of PS and chloride mediated ROS and RCS production in the oxidation
460 of S (IV) to S (VI) was shown in Fig. 5. Initially, the PS (e.g., SyrAld and VL) absorb solar
461 radiation and produce the singlet state ^{1}PS*, which then undergo a spin conversion through
462 intersystem crossing, leading to the formation of the triplet state ^{3}PS*. The ^{3}PS* can react with
463 molecular oxygen through energy transfer and generate singlet state $^1O_2$*, while the ^{3}PS* returns
464 to ground state. The $^1O_2$* can then transform to $O_2^{\bullet-}$ via electron transfer. The ^{3}PS*can also react
465 with an H donor (RH, e.g., organic acids, syringol, guaiacol, Table S3), leading to the formation
466 of alkyl or phenoxy radical (R•) and a ketyl radical (PSH•). R• can react with O_2 and form RO_2
467 radicals while PSH• can transfer an H atom to O_2 and form $HO_2^{\bullet}$, returning to its ground state
468 PS. Additionally, ^{3}PS* can react with an electron donor, e.g., Cl^-, and form chlorine radicals
469 and $PS^{\bullet-}$. The formed $PS^{\bullet-}$ then reacts with O_2 and form $O_2^{\bullet-}$, which undergoes a series of
470 reactions and form HO_2•, H_2O_2 and OH•. The above-mentioned reactions are the main processes
471 in ROS pathway. Recently, Zhang and Chan(2024) have proposed that the reactive chlorine
472 species (RCS) would contribute to sulfate formation. Cao et al. (2024) proposed a mechanism

of OH and Cl radicals formation by [Cl^--H_3O^+-O_2] under light irradiation through an electron transfer process. Our results also demonstrate that the addition of Cl^- will affect the oxidation process of S(VI) (Figures 4, S10-S12). Combining the above, the RCS pathway was shown in yellow arrows in Figure 5. The Cl• can be formed in two pathways, photoexcitation of the [Cl^--H_3O^+-O_2] complex that generates Cl radicals in deliquescent BB-NaCl droplets or aqueous BB-NaCl solution (Cao et al., 2024), and PS* mediated Cl• formation via electron transfer by Cl^- (Corral Arroyo et al., 2019). The formed Cl• can then react with each other through radical-radical reactions and produce molecular Cl_2. The Cl•$^-$can also react with Cl^- or Cl_2•$^-$, forming Cl_2•$^-$ or Cl_2. Cl• and Cl_2•$^-$ can also react with OH and form HOCl. ^{3}PS* itself can also oxidize the S(IV) (e.g., dissolved SO_2 or bisulfite) to S(VI). However, significantly lower sulfate formation was found in the presence of N_2 compared to air condition (Figure 2), highlighting the importance of secondary oxidants compared to direct PS* oxidation. As a consequence, these reactive species, e.g., OH•/HO_2•/O_2•$^-$ and Cl•/Cl_2•$^-$ may all participate in the oxidation of S(IV) to S(VI). In addition, the nitrogen-containing heterocyclic compounds such as pyrazine can act as H-bonding acceptor and facilitate the H transfer, which then generates more ROS (Dou et al., 2015). In light of the absence of substantial fluctuations in chloride concentration (Figure S13 and S14, insignificant chloride concentration change was found even in 10 ppm NaCl addition), it is postulated that chloride ions may function as a reactive medium rather than as direct reactants. In this proposed scenario, the Cl radicals and Cl_2•$^-$ intermediates generated during the reaction subsequently undergo reversion back to Cl^- ions, thereby maintaining a relatively constant Cl^- concentration throughout the experimental observations. Note that although ROS and RCS pathways both contribute to the oxidation from S(IV) to S(IV), they may act as competitive relationships due to the co-consumption of PS*. Therefore, different Cl effects may occur regarding various combinations of reactants (Figure 4, promoting effect in RS_A, inhibiting effects on RS_F).

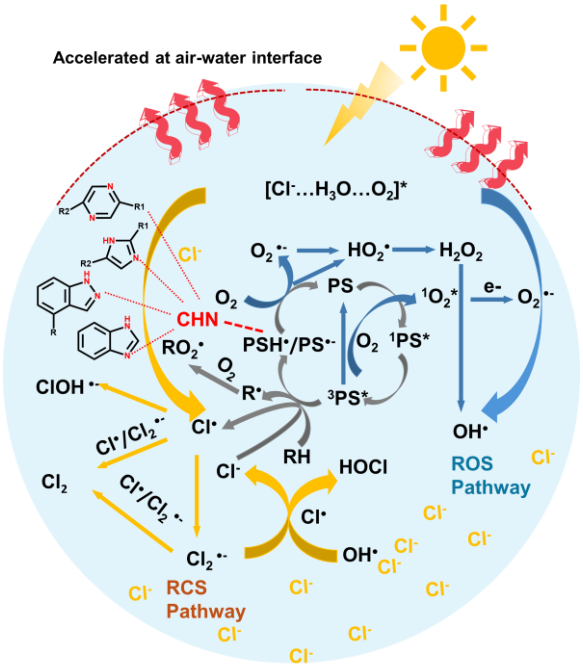

Figure 5. Conceptual diagram of PS and chloride mediated ROS and RCS production, which

participates in the oxidation processes from S(IV) to S(VI)

4 Atmospheric Implication

This study provided laboratory evidence that the PS in biomass burning extracts can enhance the sulfate formation in NaCl particles, primarily by triggering the formation of secondary oxidants under light and air, with less contribution of direct photosensitization via triplets (evidenced by N_2 atmosphere, Figure 2). The sulfate formation rate of BB_F-NaCl particles were ~10 folds higher that of IS_F-NaCl, following the trends of CS_F-NaCl>RS_F-NaCl>WS_F-NaCl>IS_F-NaCl. Upon UV exposure, the sulfate formation trends shifted to RS_A-NaCl>CS_A-NaCl>WS_A-NaCl>IS_A-NaCl, which might be explained by the effects of chloride (evidenced by aqueous reactions, Figure 4 and Table 1). Interestingly, the incorporation of Cl^-into bulk solutions increased the sulfate formation rate in RS_A, while decreased it in RS_F. This seems to be different from our group's previous work where no significant sulfate formation rate was found with the addition of Cl^- (Zhang and Chan, 2024). The difference can be explained by the following reasons: 1) differences in PS/Cl^-, the prior study might use an insufficient PS/Cl^- ratio (2:1-1:4) while the current one significantly expands it to 1:200. 2) differences in photosensitizing capacity: the former study used a strong PS, while the current study focused on the real BB (using TOC as metric, with only a small portion of TOC considered as PS). 3) the complexity of the reaction system, the former study focused on mixing two individual species, while in real BB extracts, more complicated reactions may occur. Furthermore, our results using model PS show that although additional model CHN species would increase the sulfate formation by expedited H transfer via acting as H-bond acceptor, the addition of chloride could inhibit the sulfate formation rate, suggesting that the RCS pathway was less efficient in sulfate formation compared to ROS pathway in PS-CHN bulk system (Figure S10 and S11).

Previous studies have detected a significant proportion of NOCs, including nitroaromatics (CHON) and reduced nitrogen species (CHN) in biomass burning plumes, wildfires and ambient samples (Zhong et al., 2024; Wang et al., 2017b; Song et al., 2022; Cai et al., 2020). These NOCs are considered as ubiquitous contributor to BrC, and can affect global climate and human health. Moreover, recent research has discovered aerosol pollution in marine background regions, with high levels of NOCs when air masses are transported from wildfires or biomass burning events in nearby (Zhong et al., 2024; Qin et al., 2024). These NOCs, combined with reactive gases, may mix with sea-salt aerosols and impact regional air quality in coastal zones. While our prior study has examined the potential interplay between chloride and PS at limited mixing ratios (up to 4:1 in bulk solution) (Zhang and Chan, 2024), this work expanded the Cl^-/PS ratio to a broader range (200:1) and systematically identified the interactions among different organics, including PS, NOCs, and chloride, using sulfate formation as a compass. This highlights the importance to study secondary aerosol formation in mixed experimental system under air pollution complex. Our work suggests that in coastal regions heavily influenced by anthropogenic emissions like biomass burning, especially those near the rice-growing regions or affected by transported wildfire smoke, such as Guangdong, Fujian and Taiwan, the transported BB plumes together with the high RH (Cheung et al., 2015) and abundant reactive gases, would play an inevitable role in sulfate and potentially secondary organic aerosol formation.

Data availability

Datasets are available upon request to the corresponding author, Chak K. Chan (chak.chan@kaust.edu.sa).

Author contributions

RT and CC conceptualized and designed the study. YQ and YC collected the samples. RT performed the experiments, data analysis and wrote the draft. JM provided assistance in data processing. All the authors reviewed, edited and contributed to the scientific discussions.

Competing interests

The authors declare no conflicts of interest.

Acknowledgments

We gratefully acknowledge the support from the Hong Kong Research Grants Council (No. 11314222), the National Natural Science Foundation of China (42107115), and the Natural Science Foundation of Shandong Province, China (ZR2021QD111). The authors also thank the University Research Facility in Chemical and Environmental Analysis (UCEA) at The Hong Kong Polytechnic University for the use of its UHPLC-HESI-Orbitrap Mass Spectrometer and Dr Sirius Tse and Dr Chi Hang Chow for assistance with sample analyses.

References

Alexander, B., Allman, D. J., Amos, H. M., Fairlie, T. D., Dachs, J., Hegg, D. A., and Sletten, R. S.: Isotopic constraints on the formation pathways of sulfate aerosol in the marine boundary layer of the subtropical northeast Atlantic Ocean, Journal of Geophysical Research: Atmospheres, 117, https://doi.org/10.1029/2011JD016773, 2012.

Anastasio, C. and Newberg, J. T.: Sources and sinks of hydroxyl radical in sea-salt particles, Journal of Geophysical Research: Atmospheres, 112, 2007.

Andreae, M. O.: Emission of trace gases and aerosols from biomass burning – an updated assessment, Atmos. Chem. Phys., 19, 8523-8546, 10.5194/acp-19-8523-2019, 2019.

Bond, T. C., Doherty, S. J., Fahey, D. W., Forster, P. M., Berntsen, T., DeAngelo, B. J., Flanner, M. G., Ghan, S., Kärcher, B., Koch, D., Kinne, S., Kondo, Y., Quinn, P. K., Sarofim, M. C., Schultz, M. G., Schulz, M., Venkataraman, C., Zhang, H., Zhang, S., Bellouin, N., Guttikunda, S. K., Hopke, P. K., Jacobson, M. Z., Kaiser, J. W., Klimont, Z., Lohmann, U., Schwarz, J. P., Shindell, D., Storelvmo, T., Warren, S. G., and Zender, C. S.: Bounding the role of black carbon in the climate system: A scientific assessment, Journal of Geophysical Research: Atmospheres, 118, 5380-5552, https://doi.org/10.1002/jgrd.50171, 2013.

Cai, J., Zeng, X., Zhi, G., Gligorovski, S., Sheng, G., Yu, Z., Wang, X., and Peng, P.: Molecular composition and photochemical evolution of water-soluble organic carbon (WSOC) extracted from field biomass burning aerosols using high-resolution mass spectrometry, Atmos. Chem. Phys., 20, 6115-6128, 10.5194/acp-20-6115-2020, 2020.

Calderon-Arrieta, D., Morales, A. C., Hettiyadura, A. P. S., Estock, T. M., Li, C., Rudich, Y., and Laskin, A.: Enhanced Light Absorption and Elevated Viscosity of Atmospheric Brown Carbon through

Evaporation of Volatile Components, Environmental Science & Technology, 58, 7493-7504, 10.1021/acs.est.3c10184, 2024.
Cao, Y., Liu, J., Ma, Q., Zhang, C., Zhang, P., Chen, T., Wang, Y., Chu, B., Zhang, X., Francisco, J. S., and He, H.: Photoactivation of Chlorine and Its Catalytic Role in the Formation of Sulfate Aerosols, Journal of the American Chemical Society, 146, 1467-1475, 10.1021/jacs.3c10840, 2024.
Chen, J., Li, C., Ristovski, Z., Milic, A., Gu, Y., Islam, M. S., Wang, S., Hao, J., Zhang, H., He, C., Guo, H., Fu, H., Miljevic, B., Morawska, L., Thai, P., Lam, Y. F., Pereira, G., Ding, A., Huang, X., and Dumka, U. C.: A review of biomass burning: Emissions and impacts on air quality, health and climate in China, Science of The Total Environment, 579, 1000-1034, https://doi.org/10.1016/j.scitotenv.2016.11.025, 2017.
Chen, Y., Zheng, P., Wang, Z., Pu, W., Tan, Y., Yu, C., Xia, M., Wang, W., Guo, J., Huang, D., Yan, C., Nie, W., Ling, Z., Chen, Q., Lee, S., and Wang, T.: Secondary Formation and Impacts of Gaseous Nitro-Phenolic Compounds in the Continental Outflow Observed at a Background Site in South China, Environmental Science & Technology, 56, 6933-6943, 10.1021/acs.est.1c04596, 2022.
Cheng, S.-B., Zhou, C.-H., Yin, H.-M., Sun, J.-L., and Han, K.-L.: OH produced from o-nitrophenol photolysis: A combined experimental and theoretical investigation, The Journal of chemical physics, 130, 2009.
Cheung, H. H., Yeung, M. C., Li, Y. J., Lee, B. P., and Chan, C. K.: Relative humidity-dependent HTDMA measurements of ambient aerosols at the HKUST supersite in Hong Kong, China, Aerosol Science and Technology, 49, 643-654, 2015.
Chi, J. W., Li, W. J., Zhang, D. Z., Zhang, J. C., Lin, Y. T., Shen, X. J., Sun, J. Y., Chen, J. M., Zhang, X. Y., Zhang, Y. M., and Wang, W. X.: Sea salt aerosols as a reactive surface for inorganic and organic acidic gases in the Arctic troposphere, Atmos. Chem. Phys., 15, 11341-11353, 10.5194/acp-15-11341-2015, 2015.
Corral Arroyo, P., Aellig, R., Alpert, P. A., Volkamer, R., and Ammann, M.: Halogen activation and radical cycling initiated by imidazole-2-carboxaldehyde photochemistry, Atmospheric Chemistry and Physics, 19, 10817-10828, 2019.
Dou, J., Lin, P., Kuang, B.-Y., and Yu, J. Z.: Reactive Oxygen Species Production Mediated by Humic-like Substances in Atmospheric Aerosols: Enhancement Effects by Pyridine, Imidazole, and Their Derivatives, Environmental Science & Technology, 49, 6457-6465, 10.1021/es5059378, 2015.
Fang, Z., Deng, W., Zhang, Y., Ding, X., Tang, M., Liu, T., Hu, Q., Zhu, M., Wang, Z., Yang, W., Huang, Z., Song, W., Bi, X., Chen, J., Sun, Y., George, C., and Wang, X.: Open burning of rice, corn and wheat straws: primary emissions, photochemical aging, and secondary organic aerosol formation, Atmos. Chem. Phys., 17, 14821-14839, 10.5194/acp-17-14821-2017, 2017.
Felber, T., Schaefer, T., and Herrmann, H.: Five-Membered Heterocycles as Potential Photosensitizers in the Tropospheric Aqueous Phase: Photophysical Properties of Imidazole-2-carboxaldehyde, 2-Furaldehyde, and 2-Acetylfuran, The Journal of Physical Chemistry A, 124, 10029-10039, 10.1021/acs.jpca.0c07028, 2020.
Felber, T., Schaefer, T., He, L., and Herrmann, H.: Aromatic Carbonyl and Nitro Compounds as Photosensitizers and Their Photophysical Properties in the Tropospheric Aqueous Phase, The Journal of Physical Chemistry A, 125, 5078-5095, 10.1021/acs.jpca.1c03503, 2021.
Fu, H., Ciuraru, R., Dupart, Y., Passananti, M., Tinel, L., Rossignol, S., Perrier, S., Donaldson, D. J., Chen, J., and George, C.: Photosensitized Production of Atmospherically Reactive Organic Compounds at the Air/Aqueous Interface, Journal of the American Chemical Society, 137, 8348-8351,

624 10.1021/jacs.5b04051, 2015.
625 Fushimi, A., Saitoh, K., Hayashi, K., Ono, K., Fujitani, Y., Villalobos, A. M., Shelton, B. R., Takami, A.,
626 Tanabe, K., and Schauer, J. J.: Chemical characterization and oxidative potential of particles emitted
627 from open burning of cereal straws and rice husk under flaming and smoldering conditions, Atmospheric
628 Environment, 163, 118-127, https://doi.org/10.1016/j.atmosenv.2017.05.037, 2017.
629 Gantt, B. and Meskhidze, N.: The physical and chemical characteristics of marine primary organic
630 aerosol: a review, Atmos. Chem. Phys., 13, 3979-3996, 10.5194/acp-13-3979-2013, 2013.
631 Gen, M., Zhang, R., Huang, D. D., Li, Y., and Chan, C. K.: Heterogeneous SO2 Oxidation in Sulfate
632 Formation by Photolysis of Particulate Nitrate, Environmental Science & Technology Letters, 6, 86-91,
633 10.1021/acs.estlett.8b00681, 2019a.
634 Gen, M., Zhang, R., Huang, D. D., Li, Y., and Chan, C. K.: Heterogeneous Oxidation of SO2 in Sulfate
635 Production during Nitrate Photolysis at 300 nm: Effect of pH, Relative Humidity, Irradiation Intensity,
636 and the Presence of Organic Compounds, Environmental Science & Technology, 53, 8757-8766,
637 10.1021/acs.est.9b01623, 2019b.
638 Gómez Alvarez, E., Wortham, H., Strekowski, R., Zetzsch, C., and Gligorovski, S.: Atmospheric
639 Photosensitized Heterogeneous and Multiphase Reactions: From Outdoors to Indoors, Environmental
640 Science & Technology, 46, 1955-1963, 10.1021/es2019675, 2012.
641 Guo, S. and Li, H.: Photolysis of nitrophenols in gas phase and aqueous environment: a potential daytime
642 source for atmospheric nitrous acid (HONO), Environmental Science: Atmospheres, 3, 143-155, 2023.
643 Hu, W., Zhou, H., Chen, W., Ye, Y., Pan, T., Wang, Y., Song, W., Zhang, H., Deng, W., Zhu, M., Wang,
644 C., Wu, C., Ye, C., Wang, Z., Yuan, B., Huang, S., Shao, M., Peng, Z., Day, D. A., Campuzano-Jost, P.,
645 Lambe, A. T., Worsnop, D. R., Jimenez, J. L., and Wang, X.: Oxidation Flow Reactor Results in a Chinese
646 Megacity Emphasize the Important Contribution of S/IVOCs to Ambient SOA Formation,
647 Environmental Science & Technology, 56, 6880-6893, 10.1021/acs.est.1c03155, 2022.
648 Huang, G., Wang, S., Chang, X., Cai, S., Zhu, L., Li, Q., and Jiang, J.: Emission factors and chemical
649 profile of I/SVOCs emitted from household biomass stove in China, Science of The Total Environment,
650 842, 156940, https://doi.org/10.1016/j.scitotenv.2022.156940, 2022a.
651 Huang, R.-J., Yang, L., Shen, J., Yuan, W., Gong, Y., Ni, H., Duan, J., Yan, J., Huang, H., You, Q., and
652 Li, Y. J.: Chromophoric Fingerprinting of Brown Carbon from Residential Biomass Burning,
653 Environmental Science & Technology Letters, 9, 102-111, 10.1021/acs.estlett.1c00837, 2022b.
654 Huang, S., Wu, Z., Poulain, L., van Pinxteren, M., Merkel, M., Assmann, D., Herrmann, H., and
655 Wiedensohler, A.: Source apportionment of the organic aerosol over the Atlantic Ocean from
656 53° N to 53° S: significant contributions from marine emissions and long-range transport,
657 Atmos. Chem. Phys., 18, 18043-18062, 10.5194/acp-18-18043-2018, 2018.
658 Jammoul, A., Dumas, S., D'Anna, B., and George, C.: Photoinduced oxidation of sea salt halides by
659 aromatic ketones: a source of halogenated radicals, Atmos. Chem. Phys., 9, 4229-4237, 10.5194/acp-9-
660 4229-2009, 2009.
661 Jiang, H., Carena, L., He, Y., Wang, Y., Zhou, W., Yang, L., Luan, T., Li, X., Brigante, M., Vione, D., and
662 Gligorovski, S.: Photosensitized Degradation of DMSO Initiated by PAHs at the Air-Water Interface, as
663 an Alternative Source of Organic Sulfur Compounds to the Atmosphere, Journal of Geophysical Research:
664 Atmospheres, 126, e2021JD035346, https://doi.org/10.1029/2021JD035346, 2021.
665 Jones, M. W., Abatzoglou, J. T., Veraverbeke, S., Andela, N., Lasslop, G., Forkel, M., Smith, A. J. P.,
666 Burton, C., Betts, R. A., van der Werf, G. R., Sitch, S., Canadell, J. G., Santín, C., Kolden, C., Doerr, S.
667 H., and Le Quéré, C.: Global and Regional Trends and Drivers of Fire Under Climate Change, Reviews

of Geophysics, 60, e2020RG000726, https://doi.org/10.1029/2020RG000726, 2022.
Kalogridis, A. C., Popovicheva, O. B., Engling, G., Diapouli, E., Kawamura, K., Tachibana, E., Ono, K., Kozlov, V. S., and Eleftheriadis, K.: Smoke aerosol chemistry and aging of Siberian biomass burning emissions in a large aerosol chamber, Atmospheric Environment, 185, 15-28, https://doi.org/10.1016/j.atmosenv.2018.04.033, 2018.
Kim, Y. H., Warren, S. H., Krantz, Q. T., King, C., Jaskot, R., Preston, W. T., George, B. J., Hays, M. D., Landis, M. S., and Higuchi, M.: Mutagenicity and lung toxicity of smoldering vs. flaming emissions from various biomass fuels: implications for health effects from wildland fires, Environmental health perspectives, 126, 017011, 2018.
Kim, Y. H., Warren, S. H., Kooter, I., Williams, W. C., George, I. J., Vance, S. A., Hays, M. D., Higuchi, M. A., Gavett, S. H., DeMarini, D. M., Jaspers, I., and Gilmour, M. I.: Chemistry, lung toxicity and mutagenicity of burn pit smoke-related particulate matter, Particle and Fibre Toxicology, 18, 45, 10.1186/s12989-021-00435-w, 2021.
Kipp, B. H., Faraj, C., Li, G., and Njus, D.: Imidazole facilitates electron transfer from organic reductants, Bioelectrochemistry, 64, 7-13, https://doi.org/10.1016/j.bioelechem.2003.12.010, 2004.
Koch, B. P. and Dittmar, T.: From mass to structure: An aromaticity index for high-resolution mass data of natural organic matter, Rapid communications in mass spectrometry, 20, 926-932, 2006.
Laskin, A., Laskin, J., and Nizkorodov, S. A.: Chemistry of Atmospheric Brown Carbon, Chemical Reviews, 115, 4335-4382, 10.1021/cr5006167, 2015.
Laskin, A., Smith, J. S., and Laskin, J.: Molecular Characterization of Nitrogen-Containing Organic Compounds in Biomass Burning Aerosols Using High-Resolution Mass Spectrometry, Environmental Science & Technology, 43, 3764-3771, 10.1021/es803456n, 2009.
Liang, Z., Li, Y., Go, B. R., and Chan, C. K.: Complexities of Photosensitization in Atmospheric Particles, ACS ES&T Air, 10.1021/acsestair.4c00112, 2024.
Lin, P., Rincon, A. G., Kalberer, M., and Yu, J. Z.: Elemental Composition of HULIS in the Pearl River Delta Region, China: Results Inferred from Positive and Negative Electrospray High Resolution Mass Spectrometric Data, Environmental Science & Technology, 46, 7454-7462, 10.1021/es300285d, 2012.
Lin, P., Fleming, L. T., Nizkorodov, S. A., Laskin, J., and Laskin, A.: Comprehensive Molecular Characterization of Atmospheric Brown Carbon by High Resolution Mass Spectrometry with Electrospray and Atmospheric Pressure Photoionization, Analytical Chemistry, 90, 12493-12502, 10.1021/acs.analchem.8b02177, 2018.
Liu, D., Zhang, Y., Zhong, S., Chen, S., Xie, Q., Zhang, D., Zhang, Q., Hu, W., Deng, J., Wu, L., Ma, C., Tong, H., and Fu, P.: Large differences of highly oxygenated organic molecules (HOMs) and low-volatile species in secondary organic aerosols (SOAs) formed from ozonolysis of β-pinene and limonene, Atmos. Chem. Phys., 23, 8383-8402, 10.5194/acp-23-8383-2023, 2023a.
Liu, H., Pei, X., Zhang, F., Song, Y., Kuang, B., Xu, Z., and Wang, Z.: Relative Humidity Dependence of Growth Factor and Real Refractive Index for Sea Salt/Malonic Acid Internally Mixed Aerosols, Journal of Geophysical Research: Atmospheres, 128, e2022JD037579, https://doi.org/10.1029/2022JD037579, 2023b.
Mabato, B. R. G., Li, Y. J., Huang, D. D., Wang, Y., and Chan, C. K.: Comparison of aqueous secondary organic aerosol (aqSOA) product distributions from guaiacol oxidation by non-phenolic and phenolic methoxybenzaldehydes as photosensitizers in the absence and presence of ammonium nitrate, Atmos. Chem. Phys., 23, 2859-2875, 10.5194/acp-23-2859-2023, 2023.
Mabato, B. R. G., Lyu, Y., Ji, Y., Li, Y. J., Huang, D. D., Li, X., Nah, T., Lam, C. H., and Chan, C. K.:

712 Aqueous secondary organic aerosol formation from the direct photosensitized oxidation of vanillin in the
713 absence and presence of ammonium nitrate, Atmos. Chem. Phys., 22, 273-293, 10.5194/acp-22-273-
714 2022, 2022.
715 Mao, J., Ren, X., Brune, W. H., Olson, J. R., Crawford, J. H., Fried, A., Huey, L. G., Cohen, R. C., Heikes,
716 B., Singh, H. B., Blake, D. R., Sachse, G. W., Diskin, G. S., Hall, S. R., and Shetter, R. E.: Airborne
717 measurement of OH reactivity during INTEX-B, Atmos. Chem. Phys., 9, 163-173, 10.5194/acp-9-163-
718 2009, 2009.
719 Mohr, C., Lopez-Hilfiker, F. D., Zotter, P., Prévôt, A. S. H., Xu, L., Ng, N. L., Herndon, S. C., Williams,
720 L. R., Franklin, J. P., Zahniser, M. S., Worsnop, D. R., Knighton, W. B., Aiken, A. C., Gorkowski, K. J.,
721 Dubey, M. K., Allan, J. D., and Thornton, J. A.: Contribution of Nitrated Phenols to Wood Burning Brown
722 Carbon Light Absorption in Detling, United Kingdom during Winter Time, Environmental Science &
723 Technology, 47, 6316-6324, 10.1021/es400683v, 2013.
724 Parker, K. M. and Mitch, W. A.: Halogen radicals contribute to photooxidation in coastal and estuarine
725 waters, Proceedings of the National Academy of Sciences, 113, 5868-5873, 2016.
726 Peng, Z. and Jimenez, J. L.: Radical chemistry in oxidation flow reactors for atmospheric chemistry
727 research, Chemical Society Reviews, 49, 2570-2616, 2020.
728 Pozzoli, L., Gilardoni, S., Perrone, M. G., de Gennaro, G., de Rienzo, M., and Vione, D.: POLYCYCLIC
729 AROMATIC HYDROCARBONS IN THE ATMOSPHERE: MONITORING, SOURCES, SINKS AND
730 FATE. I: MONITORING AND SOURCES, Annali di Chimica, 94, 17-33,
731 https://doi.org/10.1002/adic.200490002, 2004.
732 Qin, Y., Wang, H., Wang, Y., Lu, X., Tang, H., Zhang, J., Li, L., and Fan, S.: Wildfires in Southeast Asia
733 pollute the atmosphere in the northern South China Sea, Science Bulletin, 69, 1011-1015,
734 https://doi.org/10.1016/j.scib.2024.02.026, 2024.
735 Qiu, Y., Wu, X., Zhang, Y., Xu, L., Hong, Y., Chen, J., Chen, X., and Deng, J.: Aerosol light absorption
736 in a coastal city in Southeast China: Temporal variations and implications for brown carbon, Journal of
737 Environmental Sciences, 80, 257-266, https://doi.org/10.1016/j.jes.2019.01.002, 2019.
738 Rowe, J. P., Lambe, A. T., and Brune, W. H.: Technical Note: Effect of varying the λ = 185 and
739 254 nm photon flux ratio on radical generation in oxidation flow reactors, Atmos. Chem. Phys.,
740 20, 13417-13424, 10.5194/acp-20-13417-2020, 2020.
741 Safiarian, M. S., Ugboya, A., Khan, I., Marichev, K. O., and Grant, K. B.: New Insights into the
742 Phototoxicity of Anthracene-Based Chromophores: The Chloride Salt Effect, Chemical Research in
743 Toxicology, 36, 1002-1020, 10.1021/acs.chemrestox.2c00235, 2023.
744 Salvador, C. M. G., Tang, R., Priestley, M., Li, L. J., Tsiligiannis, E., Le Breton, M., Zhu, W., Zeng, L.,
745 Wang, H., and Yu, Y.: Ambient nitro-aromatic compounds–biomass burning versus secondary formation
746 in rural China, Atmospheric Chemistry and Physics Discussions, 2020, 1-36, 2020.
747 Sangwan, M. and Zhu, L.: Absorption cross sections of 2-nitrophenol in the 295–400 nm region and
748 photolysis of 2-nitrophenol at 308 and 351 nm, The Journal of Physical Chemistry A, 120, 9958-9967,
749 2016.
750 Sangwan, M. and Zhu, L.: Role of Methyl-2-nitrophenol Photolysis as a Potential Source of OH Radicals
751 in the Polluted Atmosphere: Implications from Laboratory Investigation, The Journal of Physical
752 Chemistry A, 122, 1861-1872, 10.1021/acs.jpca.7b11235, 2018.
753 Song, J., Li, M., Zou, C., Cao, T., Fan, X., Jiang, B., Yu, Z., Jia, W., and Peng, P. a.: Molecular
754 Characterization of Nitrogen-Containing Compounds in Humic-like Substances Emitted from Biomass
755 Burning and Coal Combustion, Environmental Science & Technology, 56, 119-130,

10.1021/acs.est.1c04451, 2022.
Song, K., Tang, R., Li, A., Wan, Z., Zhang, Y., Gong, Y., Lv, D., Lu, S., Tan, Y., Yan, S., Yan, S., Zhang, J., Fan, B., Chan, C. K., and Guo, S.: Particulate organic emissions from incense-burning smoke: Chemical compositions and emission characteristics, Science of The Total Environment, 897, 165319, https://doi.org/10.1016/j.scitotenv.2023.165319, 2023.
Tang, R., Zhang, R., Ma, J., Song, K., Mabato, B. R. G., Cuevas, R. A. I., Zhou, L., Liang, Z., Vogel, A. L., Guo, S., and Chan, C. K.: Sulfate Formation by Photosensitization in Mixed Incense Burning–Sodium Chloride Particles: Effects of RH, Light Intensity, and Aerosol Aging, Environmental Science & Technology, 57, 10295-10307, 10.1021/acs.est.3c02225, 2023.
Ting, Y., Mitchell, E. J. S., Allan, J. D., Liu, D., Spracklen, D. V., Williams, A., Jones, J. M., Lea-Langton, A. R., McFiggans, G., and Coe, H.: Mixing State of Carbonaceous Aerosols of Primary Emissions from "Improved" African Cookstoves, Environmental Science & Technology, 52, 10134-10143, 10.1021/acs.est.8b00456, 2018.
Tkacik, D. S., Lambe, A. T., Jathar, S., Li, X., Presto, A. A., Zhao, Y., Blake, D., Meinardi, S., Jayne, J. T., Croteau, P. L., and Robinson, A. L.: Secondary Organic Aerosol Formation from in-Use Motor Vehicle Emissions Using a Potential Aerosol Mass Reactor, Environmental Science & Technology, 48, 11235-11242, 10.1021/es502239v, 2014.
van Pinxteren, M., Fiedler, B., van Pinxteren, D., Iinuma, Y., Körtzinger, A., and Herrmann, H.: Chemical characterization of sub-micrometer aerosol particles in the tropical Atlantic Ocean: marine and biomass burning influences, Journal of Atmospheric Chemistry, 72, 105-125, 10.1007/s10874-015-9307-3, 2015.
Wang, K., Zhang, Y., Tong, H., Han, J., Fu, P., Huang, R.-J., Zhang, H., and Hoffmann, T.: Molecular-Level Insights into the Relationship between Volatility of Organic Aerosol Constituents and PM2.5 Air Pollution Levels: A Study with Ultrahigh-Resolution Mass Spectrometry, Environmental Science & Technology, 58, 7947-7957, 10.1021/acs.est.3c10662, 2024a.
Wang, N., Zhou, D., Liu, H., Tu, Y., Ma, Y., and Li, Y.: Triplet-Excited Dissolved Organic Matter Efficiently Promoted Atmospheric Sulfate Production: Kinetics and Mechanisms, Separations, 10, 335, 2023a.
Wang, S., Liu, T., Jang, J., Abbatt, J. P. D., and Chan, A. W. H.: Heterogeneous interactions between SO2 and organic peroxides in submicron aerosol, Atmos. Chem. Phys., 21, 6647-6661, 10.5194/acp-21-6647-2021, 2021.
Wang, T., Deng, L., Tan, C., Hu, J., and Singh, R. P.: Comparative analysis of chlorinated disinfection byproducts formation from 4-nitrophenol and 2-amino-4-nitrophenol during UV/post-chlorination, Science of The Total Environment, 927, 172200, https://doi.org/10.1016/j.scitotenv.2024.172200, 2024b.
Wang, X., Gu, R., Wang, L., Xu, W., Zhang, Y., Chen, B., Li, W., Xue, L., Chen, J., and Wang, W.: Emissions of fine particulate nitrated phenols from the burning of five common types of biomass, Environmental Pollution, 230, 405-412, https://doi.org/10.1016/j.envpol.2017.06.072, 2017a.
Wang, X., Gemayel, R., Hayeck, N., Perrier, S., Charbonnel, N., Xu, C., Chen, H., Zhu, C., Zhang, L., Wang, L., Nizkorodov, S. A., Wang, X., Wang, Z., Wang, T., Mellouki, A., Riva, M., Chen, J., and George, C.: Atmospheric Photosensitization: A New Pathway for Sulfate Formation, Environmental Science & Technology, 54, 3114-3120, 10.1021/acs.est.9b06347, 2020a.
Wang, Y., Hu, M., Xu, N., Qin, Y., Wu, Z., Zeng, L., Huang, X., and He, L.: Chemical composition and light absorption of carbonaceous aerosols emitted from crop residue burning: influence of combustion efficiency, Atmos. Chem. Phys., 20, 13721-13734, 10.5194/acp-20-13721-2020, 2020b.
Wang, Y., Qiu, T., Zhang, C., Hao, T., Mabato, B. R. G., Zhang, R., Gen, M., Chan, M. N., Huang, D. D.,

and Ge, X.: Co-photolysis of mixed chromophores affects atmospheric lifetimes of brown carbon, Environmental Science: Atmospheres, 3, 1145-1158, 2023b.
Wang, Y., Hu, M., Lin, P., Guo, Q., Wu, Z., Li, M., Zeng, L., Song, Y., Zeng, L., Wu, Y., Guo, S., Huang, X., and He, L.: Molecular Characterization of Nitrogen-Containing Organic Compounds in Humic-like Substances Emitted from Straw Residue Burning, Environmental Science & Technology, 51, 5951-5961, 10.1021/acs.est.7b00248, 2017b.
Wu, C.-H., Yuan, C.-S., Yen, P.-H., Yeh, M.-J., and Soong, K.-Y.: Diurnal and seasonal variation, chemical characteristics, and source identification of marine fine particles at two remote islands in South China Sea: A superimposition effect of local emissions and long-range transport, Atmospheric Environment, 270, 118889, https://doi.org/10.1016/j.atmosenv.2021.118889, 2022.
Xie, M., Chen, X., Hays, M. D., and Holder, A. L.: Composition and light absorption of N-containing aromatic compounds in organic aerosols from laboratory biomass burning, Atmos. Chem. Phys., 19, 2899-2915, 10.5194/acp-19-2899-2019, 2019.
Yang, M., Zhang, H., Chang, F., and Hu, X.: Self-sensitized photochlorination of benzo[a]pyrene in saline water under simulated solar light irradiation, Journal of Hazardous Materials, 408, 124445, https://doi.org/10.1016/j.jhazmat.2020.124445, 2021.
Yao, M., Zhao, Y., Hu, M., Huang, D., Wang, Y., Yu, J. Z., and Yan, N.: Multiphase reactions between secondary organic aerosol and sulfur dioxide: kinetics and contributions to sulfate formation and aerosol aging, Environmental Science & Technology Letters, 6, 768-774, 2019.
Ye, C., Lu, K., Song, H., Mu, Y., Chen, J., and Zhang, Y.: A critical review of sulfate aerosol formation mechanisms during winter polluted periods, Journal of Environmental Sciences, 123, 387-399, https://doi.org/10.1016/j.jes.2022.07.011, 2023.
Ye, J., Abbatt, J. P., and Chan, A. W.: Novel pathway of SO 2 oxidation in the atmosphere: reactions with monoterpene ozonolysis intermediates and secondary organic aerosol, Atmospheric Chemistry and Physics, 18, 5549-5565, 2018.
Zhang, L., Hu, B., Liu, X., Luo, Z., Xing, R., Li, Y., Xiong, R., Li, G., Cheng, H., Lu, Q., Shen, G., and Tao, S.: Variabilities in Primary N-Containing Aromatic Compound Emissions from Residential Solid Fuel Combustion and Implications for Source Tracers, Environmental Science & Technology, 56, 13622-13633, 10.1021/acs.est.2c03000, 2022.
Zhang, R. and Chan, C. K.: Simultaneous formation of sulfate and nitrate via co-uptake of SO 2 and NO 2 by aqueous NaCl droplets: combined effect of nitrate photolysis and chlorine chemistry, Atmospheric Chemistry and Physics, 23, 6113-6126, 2023a.
Zhang, R. and Chan, C. K.: Simultaneous formation of sulfate and nitrate via co-uptake of SO2 and NO2 by aqueous NaCl droplets: combined effect of nitrate photolysis and chlorine chemistry, Atmos. Chem. Phys., 23, 6113-6126, 10.5194/acp-23-6113-2023, 2023b.
Zhang, R. and Chan, C. K.: Enhanced Sulfate Formation through Synergistic Effects of Chlorine Chemistry and Photosensitization in Atmospheric Particles, ACS ES&T Air, 1, 92-102, 10.1021/acsestair.3c00030, 2024.
Zhang, R., Gen, M., Huang, D., Li, Y., and Chan, C. K.: Enhanced Sulfate Production by Nitrate Photolysis in the Presence of Halide Ions in Atmospheric Particles, Environmental Science & Technology, 54, 3831-3839, 10.1021/acs.est.9b06445, 2020a.
Zhang, S., Li, D., Ge, S., Wu, C., Xu, X., Liu, X., Li, R., Zhang, F., and Wang, G.: Elucidating the Mechanism on the Transition-Metal Ion-Synergetic-Catalyzed Oxidation of SO2 with Implications for Sulfate Formation in Beijing Haze, Environmental Science & Technology, 58, 2912-2921,

10.1021/acs.est.3c08411, 2024.
Zhang, S., Li, D., Ge, S., Liu, S., Wu, C., Wang, Y., Chen, Y., Lv, S., Wang, F., Meng, J., and Wang, G.: Rapid sulfate formation from synergetic oxidation of SO2 by O3 and NO2 under ammonia-rich conditions: Implications for the explosive growth of atmospheric PM2.5 during haze events in China, Science of The Total Environment, 772, 144897, https://doi.org/10.1016/j.scitotenv.2020.144897, 2021a.
Zhang, T., Dong, J., Zhang, C., Kong, D., Ji, Y., Zhou, Q., and Lu, J.: Photo-transformation of acetaminophen sensitized by fluoroquinolones in the presence of bromide, Chemosphere, 327, 138525, https://doi.org/10.1016/j.chemosphere.2023.138525, 2023.
Zhang, Y., Wang, K., Tong, H., Huang, R.-J., and Hoffmann, T.: The maximum carbonyl ratio (MCR) as a new index for the structural classification of secondary organic aerosol components, Rapid Communications in Mass Spectrometry, 35, e9113, https://doi.org/10.1002/rcm.9113, 2021b.
Zhang, Y., Bao, F., Li, M., Xia, H., Huang, D., Chen, C., and Zhao, J.: Photoinduced Uptake and Oxidation of SO2 on Beijing Urban PM2.5, Environmental Science & Technology, 54, 14868-14876, 10.1021/acs.est.0c01532, 2020b.
Zhao, R., Zhang, Q., Xu, X., Wang, W., Zhao, W., Zhang, W., and Zhang, Y.: Effect of photooxidation on size distribution, light absorption, and molecular compositions of smoke particles from rice straw combustion, Environmental Pollution, 311, 119950, https://doi.org/10.1016/j.envpol.2022.119950, 2022.
Zherebker, A., Rukhovich, G. D., Sarycheva, A., Lechtenfeld, O. J., and Nikolaev, E. N.: Aromaticity Index with Improved Estimation of Carboxyl Group Contribution for Biogeochemical Studies, Environmental Science & Technology, 56, 2729-2737, 10.1021/acs.est.1c04575, 2022.
Zhong, S., Liu, R., Yue, S., Wang, P., Zhang, Q., Ma, C., Deng, J., Qi, Y., Zhu, J., and Liu, C.-Q.: Peatland Wildfires Enhance Nitrogen-Containing Organic Compounds in Marine Aerosols over the Western Pacific, Environmental Science & Technology, 2024.
Zhou, L., Liang, Z., Mabato, B. R. G., Cuevas, R. A. I., Tang, R., Li, M., Cheng, C., and Chan, C. K.: Sulfate formation via aerosol-phase SO2 oxidation by model biomass burning photosensitizers: 3,4-dimethoxybenzaldehyde, vanillin and syringaldehyde using single-particle mixing-state analysis, Atmos. Chem. Phys., 23, 5251-5261, 10.5194/acp-23-5251-2023, 2023.